Space Charge Induced Surface Stresses: Implications in Ceria and Other Ionic Solids

Brian W. Sheldon and Vivek B. Shenoy

Phys. Rev. Lett. **106**, 216104 — Published 27 May 2011

DOI: 10.1103/PhysRevLett.106.216104

Space charge induced surface stresses: implications in ceria and other ionic solids

Brian W. Sheldon and Vivek B. Shenoy

School of Engineering, Brown University, Providence, RI 02912

Volume changes associated with point defects in space charge layers can produce strains that substantially alter thermodynamic equilibrium near surfaces in ionic solids. For example, near-surface compressive stresses exceeding -10 GPa are predicted for ceria. The magnitude of this effect is consistent with anomalous lattice parameter increases that occur in ceria nanoparticles. These stresses should significantly alter defect concentrations and key transport properties in a wide range of materials (e.g., ceria electrolytes in fuel cells).

Space charge models are widely used to describe the electrochemical behavior of surfaces and interfaces in ionic solids [1-11]. The premise for these descriptions is that defect formation energies at surfaces differ from those in the bulk. This leads to an electric potential gradient near the surface, to maintain thermodynamic equilibrium. Fig 1 shows the regions associated with this phenomenon near a simple surface. In the standard analysis, surface defect energies are reflected only in the total electric potential difference between the surface and bulk, and the description focuses on evaluating defect concentration variations across a space charge (SC) layer. The standard analysis also ignores the volume changes that should be associated with these defect concentration variations. This expansion or contraction is constrained by the bulk crystal, and can thus induce a corresponding compositional stress in the SC region. Extending the standard SC treatment to incorporate these stresses is the primary objective of this letter.

Stresses in the SC layer should significantly influence surface-related properties. To demonstrate this with a meaningful example, our analysis focuses on $CeO_{2-\chi}$ which is used as a fuel cell electrolyte and a catalyst. Stresses induced by non-stoichiometry in ceria are documented [12-15], and in polycrystalline ceria it is widely believed that SC effects at grain

boundaries lead to substantial variations in ionic and electrical conductivity [5,16,17]. In particular, SC induced decreases in ionic conductivity are a critical limitation in fuel cell electrolytes. Several recent reports also suggest that stresses associated with ceria interfaces may increase ionic conductivity [18-20].

Ceria exhibits substantial nonstoichiometry. Oxygen vacancies dominate the defect chemistry [21-25], with oxygen removal given by:

$$O_O + 2Ce_{Ce} \;\; \rightleftarrows \;\; V_O^{\cdot\cdot} + 2\,Ce'_{Ce} + \frac{1}{2}\,O_2(g) \tag{1}$$

where $V_O^{\cdot\cdot}$ are oxygen vacancies and Ce'_{Ce} is Ce^{3+}on a Ce^{4+} site (i.e., an extra electron). Analogous expressions for other non-stoichiometric crystals include cation deficiencies, interstitial defects, etc. The key feature here is dominant defects with net positive and negative charges (e.g., $V_O^{\cdot\cdot}$ and Ce'_{Ce} in Eq 1). The non-stoichiometry in Eq 1 produces significant volume changes in $\mathrm{CeO}_{2-\chi}$[23,24], however, the implications of these changes on stress in the SC layer have not been evaluated. The key thermodynamic property here is the partial molar volume of oxygen:

$$\overline{V_O} \;=\; \left(\frac{\partial V}{\partial N_O}\right)_{T,P,N_C} \tag{2}$$

where V is the total volume and N_O and N_C are the numbers of anions and cations. This quantity describes volume change in the bulk, however, point defect variations in the SC layer should produce different volume changes and thus give rise to stress. Here, it is necessary to separate the partial molar volumes for $V_O^{\cdot\cdot}$ and Ce'_{Ce} into $\overline{V_V}$ and $\overline{V_e}$. With a fixed number of cations, the following basic relationship follows from Eqs 1 and 2:

$$dV = \; \overline{V_O}\, dN_O \; = \; \overline{V_V}\, dN_V + \; \overline{V_e}\, dN_e \tag{3}$$

In the bulk crystal, electric neutrality associated with $V_O^{\cdot\cdot}$ and Ce'_{Ce}requires that $dN_e = 2\, dN_V = -2\, dN_O$. Combining this with Eq 3 then gives:

$$\overline{V_O} \;=\; -\,\overline{V_V} \;-\; 2\,\overline{V_e} \tag{4}$$

In the bulk separating $\overline{V_O}$ into the two components in Eq 4 is unnecessary because of electric neutrality. However local neutrality does not hold in the SC layer, and thus $\overline{V_V}$ and $\overline{V_e}$ should be treated as separate contributions.

We initially assume that the SC layer behaves like a thin film on a thick substrate. With isotropic linear elastic behavior, the SC layer stress is biaxial, with $\sigma(z) = \sigma_{xx} = \sigma_{yy}$ and $\sigma_{zz} = 0$. The relationship between σ and the point defects is then given by:

$$\sigma(z) \;=\; -M([f_V(z) - f_V^{\infty}] \;+\; [f_e(z) - f_e^{\infty}]) \tag{5}$$

where *M* is the biaxial modulus. The f's are linear strains due to the compositionally induced expansion, where ∞ refers to bulk values. Total strain is divided into oxygen vacancy (subscript *V*) and extra electron (subscript *e*) contributions, following Eq 1. With expected strains $<$ ~1%:

$$f_i(z) - f_i^{\infty} \;\cong\; \frac{2}{3\,V_m} \int_{c_i^{\infty}}^{c_i} \overline{V_i}\, dc_i \tag{6}$$

where V_m is the molar volume of stoichiometric ceria, i refers to either *V* or *e*, and the *c's* are mole fractions (normalized to the number of O lattice sites). Assuming further that $\overline{V_V}$ and $\overline{V_e}$ are constants (valid for dilute solutions), then Eqs 5 – 6 can be combined to give:

$$\sigma(z) = -(2M/3V_m)\,[\overline{V_V}\,(c_V(z) - c_V^{\infty}) + \overline{V_e}\,(c_e(z) - c_e^{\infty})] \tag{7}$$

Existing SC models are based on thermodynamic equilibrium, however, they do not incorporate strain energies. To include this, we start with a thermodynamic potential, Γ_i, that includes both elastic and electric field effects:

$$\Gamma_i = \mu_i^o + RT \ln a_i + z_i\, \mathcal{F}\, \phi \;-\frac{1}{3}\overline{V_i}\,\sigma_{jj} \tag{8}$$

where μ_i^o and a_i are the reference chemical potential and the activity of species i. The third term on the right side is the contribution from the electric potential, ϕ, where $\mathcal{F}$ is Faraday's constant and z_i is the valence. The last term describes elastic effects. An additional elastic contribution should be added to Eq 8 if *M* varies with composition. However, this can be neglected in ceria, because O vacancy concentrations in the SC layer are small even when χ is large in the bulk (experiments show essentially constant *M* for small χ [26]). The present analysis demonstrates that the remaining elastic term in Eq 8 can have a significant impact.

Thermodynamic equilibrium across the SC layer corresponds to equating Γ_i 's between the surface region and the bulk. Again assuming dilute solutions, this gives:

$$c_V(z) = \;\chi \exp\left[\frac{2\,\overline{V_V}}{3\,RT}\sigma(z)\right] \exp\left[-\frac{2\mathcal{F}}{RT}\Delta\phi(z)\right] \tag{9a}$$

$$c_e(z) = c_e^{\infty} \exp\left[\frac{2\,\overline{V}_e}{3\,RT}\sigma(z)\right] \exp\left[\frac{\mathcal{F}}{RT}\Delta\phi(z)\right] \tag{9b}$$

where $\Delta\phi(z) = \phi(z) - \phi^{\infty}$, and χ is the bulk nonstoichiometry (i.e., in $CeO_{2-\chi}$). Because χ specifies the bulk composition, it is appropriate to use χ in place of c_V^{∞} in Eq 9a when vacancies are the dominant point defect (i.e., each missing O corresponds to a vacancy). The results in Eq 9 are identical to the standard model, except for the added stress term.

The potential difference across the space charge layer can then be evaluated by solving the Poisson-Boltzmann equation, given in one dimension by:

$$\frac{d^2\Delta\phi}{dz^2} = -\frac{2\,\mathcal{F}}{\xi\,V_m}(2c_V - c_e) \tag{10}$$

where ξ is the dielectric permittivity. The standard boundary conditions are:

$$\Delta\phi(0) = \Delta\phi_o \quad \text{and} \quad \Delta\phi(\infty) = 0 \tag{11}$$

which correspond to equilibrium with the surface at z = 0 (i.e., a fixed potential), and to the properties of the bulk crystal at $z \to \infty$.

A complete description of the defect concentrations and hence the stress across the layer is provided by Eqs 8 – 11. It is convenient to rescale this model in terms of normalized defect concentrations:

$$\frac{d^2\hat{\phi}}{dz^2} = \frac{\chi}{\lambda^2}(\hat{c}_e - \hat{c}_V) \tag{12a}$$

$$\hat{c}_V(z) = \exp\left[-2\hat{\phi} - 2\,\chi\,\alpha\,\beta(\beta[\hat{c}_V - 1] - (1+\beta)[\hat{c}_e - 1])\right] \tag{12b}$$

$$\hat{c}_e(z) = \exp\left[\hat{\phi} + \chi\,\alpha\,(1+\beta)(\beta[\hat{c}_V - 1] - (1+\beta)[\hat{c}_e - 1])\right] \tag{12c}$$

$$\hat{\phi}(0) = \hat{\phi}_o \quad \text{and} \quad \hat{\phi}(\infty) = 0 \tag{12d}$$

where:

$$\lambda = \frac{\sqrt{\xi\,V_m(RT)}}{2\,\mathcal{F}};\ \hat{\phi} = \frac{\mathcal{F}\,\Delta\phi}{RT};\ \hat{c}_e = \frac{c_e}{c_e^{\infty}};\ \hat{c}_V = \frac{c_V}{\chi};\ \alpha = \frac{2\,M\,\overline{V_O}^2}{9\,RT\,V_m};\ \beta = \frac{\overline{V_V}}{\overline{V_O}} = -1 - \frac{2\,\overline{V}_e}{\overline{V_O}} \tag{12e}$$

If values of α and β are specified, Eq 12 can be solved to obtain the defect and stress concentrations across the SC layer, for different values of χ and the boundary condition, $\hat{\phi}_o$. Most of the quantities in Eq 12 are known physical properties. For ceria $\overline{V_O}$ is known from experiments, and thus α can be calculated. However, it is difficult to directly measure the volume changes for the individual defects, $\overline{V_V}$ and $\overline{V_e}$. Only one of these values is needed to determine β, since the other can be obtained with Eq 4. A simple estimate of $\overline{V_e}$ is used here, based on the 18% increase in ionic radius between Ce^{3+} and Ce^{4+}. A fluorite unit cell with Ce^{3+} replacing Ce^{4+} then corresponds to $\overline{V_e}$ = 5.46 cm^3/mole, which leads to β = 2.7.

Calculated profiles obtained by solving Eq 12 numerically are shown in Fig 1. The impact of stress is clearly significant here, based on comparisons with the conventional SC model (i.e., the dotted lines obtained without stress). For a given set of conditions, the maximum stress occurs at the surface ($\sigma(0)$), and then decreases as one moves towards the bulk. The calculated values of $\sigma(0)$ in Fig 2a demonstrate that variations in the defect concentrations in the SC layer can produce substantial stresses. Contours showing fixed values of $\sigma(0)$ are also shown in Fig 2b, as a function of $\Delta\phi_o$ and χ. The impact of these stresses on the predicted values of $\hat{c}_e(0)$ then follows directly from Eq 9b. For example, at 1073 K stresses of $\sigma(0)$ = -1 GPa and -10 GPa decrease $\hat{c}_e(0)$ by 47.1% and 99.8% respectively (equivalent to $\Delta\phi_o$ decreases of 0.06 V and 0.6 V). Thus the stress impact is significant for most of the range shown in Fig 2b. While negative values of $\Delta\phi_o$ lead to similar tensile stresses in the SC layer, these values are not shown here, primarily because existing experimental evidence corresponds to positive $\Delta\phi_o$ values for pure ceria.

When the underlying crystal is much thicker than h_{SC}, integrating over$\sigma(z)$ gives:

$$\Sigma_{SC} = \int_0^\infty \sigma(z)\, dz = \frac{2\, M\, \overline{V_O}}{3\, V_m}\, \chi \int_0^\infty \left[(1+\beta)[\hat{c}_e - 1] - \beta[\hat{c}_V - 1]\right] dz \qquad (13)$$

As seen in Fig. 1, h_{SC} is typically two to three times the Debye length, $\lambda/\sqrt{\chi}$. Because this is typically on the nm scale, Σ_{SC} can often be viewed as a contribution to the surface stress. The total effective surface stress is then $\Sigma_S = \Sigma_S^o + \Sigma_{SC}$, where Σ_S^o is the conventional value associated with the actual surface atoms. The results in Fig 3 were obtained with Eq. 13, based on numerical solutions to Eq. 12 at *T*= 1073 K (since ceria defect chemistry is usually studied at

elevated temperature). This SC contribution to the surface stress is negative because of the volume expansion associated with Ce^{3+} ions. Since the magnitude of Σ_S^o is generally comparable to surface free energies, the larger values of Σ_{SC} that are predicted in some regions of Fig 3 will dominate the surface stress.

Ceria nanoparticles provide a basis for comparing experimental results to the predicted compressive surface stresses. A number of researchers have observed significant increases in the lattice parameter, a, as the particle radius, r, decreases [27-33]. This has been attributed to volume expansions induced by Ce^{3+} ions, which is consistent with experiments showing higher Ce^{3+} concentrations as r decreases [28,31,32]. Higher Ce^{3+} levels have also been observed near particle surfaces [31], which is generally consistent with SC models.

A relatively simple estimate of lattice parameter changes in small spherical particles can be obtained from the Laplace pressure:

$$\Delta P = \frac{2\,\Sigma_S}{r} \cong -\left(\frac{E}{1-2\nu}\right)\frac{(a - a_o)}{a_o} \qquad (14)$$

where a_o is the unstrained lattice parameter, E is Young's modulus, and ν is Poisson's ratio. In most materials, $\Sigma_S^o > 0$ (tensile surface stress) imposes compressive stress on the particles and reduces a. This kind of comparison between nanocrystal lattice parameters and Σ_S for planar surfaces generally gives good agreement [34]. The negative Σ_S values in ceria due to SC contributions are thus potentially consistent with the experimentally observed increases in a. To estimate the average strain note that the direct lattice expansion due to Ce^{3+} ions inside the SC layer is not accounted for in Eq 14. This additional contribution can be estimated as $-\Sigma_{SC} / M\, h_{SC}$. Combining this with the strain induced by surface stress (Eq 14), and using r = 7.5 nm and Σ_S = -5 J/m^2 predicts a 0.6% increase in a. Experiments with this particle size report increases of 0.3–0.8% [27-32], which is very good agreement with our model given the nature of this simple comparison. A more precise assessment is difficult because the oxygen activity in these experiments is not reported (i.e., χ is unknown). At even smaller particle sizes a number of researchers have reported larger lattice parameter increases [27-33] which are also nominally consistent with large compressive surface stresses. However, the Laplace pressure approximation in Eq. 14 is only reasonable if the SC layer thickness is much smaller than r. Even at r = 7.5 nm this approximation could be questioned (depending on the exact values of $\Delta\phi_o$

and χ). As *r* decreases, the analysis leading to Eq 12 should be modified to properly evaluate the stress field in small particles.

In principle, experiments with single crystal films could also be compared directly to the model in Eq 12. However, we are not aware of any direct measurements of this type. In polycrystalline titania and ceria films, significant compositional stresses due to grain boundaries have been reported [15,35]. These effects are consistent with the proposed SC layer stresses, however, direct quantitative analysis of grain boundaries requires a more sophisticated model than Eq 12.

In summary, the principle finding presented here is that near-surface variations in point defects can induce stresses that are large enough to significantly alter thermodynamic equilibrium. These effects have generally been neglected in standard space charge models. The predicted local compressive stresses in $CeO_{2-\chi}$ are large enough to dominate the effective surface stress, and the estimated values are consistent with the large anomalous lattice expansions that have been observed experimentally in ceria and other oxide nanoparticles. This modified space charge analysis is directly applicable to a wide variety of non-stoichiometric ionic solids. Similar effects should also occur at grain boundaries and other solid-solid interfaces, where proper treatment of the stress fields requires a modified analysis. In general, negative surface stresses of several J/m^2 are large enough to significantly alter important surface and grain boundaries properties such as dopant solubilities and ion diffusivities. Hopefully these predictions will motivate more detailed investigations of these effects.

This work was funded by NSF (primary support from DMR-0805172, VBS also acknowledges DMS-0854919 and DMS-0914648).

References

1. K.L. Kliewer and J.S. Koehler, *Phys. Rev*. **140**, A 1226 (1965).
2. J. Maier, *Prog. Solid State Chem* **23**, 171 (1993).
3. J.A.S. Ikeda and Y.-M. Chiang, *J. Am. Ceram. Soc*., **76**, 2437 (1993).
4. A. Tschope, *Solid State Ionics* **139** , 267 (2001).
5. I. Lubomirsky, J. Fleig, and J. Maier, *J. Appl. Phys.* **92**, 6819 (2002).
6. J. Chen *et al.*, *Phys. Rev. Lett*. **95**, 256103 (2005).
7. J. Jamnik, *Solid State Ionics* **177**, 2543 (2006).
8. D.R. Khanal and J. Wu, *Nano Letters* **7**, 2278 (2007).
9. F. Rettig and R. Moos, *Solid State Ionics* **179** , 2299 (2008).
10. S.J. Litzelman *et al*, *J. Electroceram* **22**, 405(2009).
11. C. Kjlseth *et al.*, *Sol State Ionics* **181**, 268 (2010).
12. A. Atkinson, *Solid State Ionics*, **95**, 249 (1997).
13. R. Krishnamurthy and B. W. Sheldon, *Acta Mater.*, **52**, 1807 (2004).
14. M. Greenberg *et al*, *Adv. Funct. Mater.* **16**, 48 (2006).
15. S. Mandowara and B.W. Sheldon, *ECS Trans* **11 (33)**, 191 (2008).
16. S. Kim and J. Maier, *J. Electrochem. Soc*. **149**, J73 (2002).
17. P. Knauth, *Solid State Ionics* **177**, 2495 (2006).
18. S. Azad *et al*, *Appl. Phys. Lett*. **86**, 131096 (2005).
19. X. Guo and J. Maier, *Adv. Mater.* **21**, 2619 (2009).
20. S. Sanna *et al.*, *Small* **6**, 1863 (2010).
21. B.C.H. Steele and J.M. Floyd, *Proc. Br. Ceram. Soc*. **19**, 55 (1971).
22. J. Faber, M.A. Seitz, and M.H. Mueller, *J. Phys. Chem. Solids* **37**, 903 (1975).
23. M. Mogensen, N.M. Sammes, and G.A. Tompsett, *Solid State Ionics* **129**, 63 (2000).
24. S.R. Bishop, K.L. Duncan, and E.D. Wachsman, *Acta. Mater.* **57**, 3596 (2009).
25. F.C. Larche and J.W. Cahn, *Acta Met*. **33**, 331 (1985).
26. Y. Wang *et al.*, *Solid State Ionics* **178**, 53 (2007).
27. S. Tsunekawa *Nanostr. Mater*. **11**, 141 (1999).
28. S. Tsunekawa *et al.*, *Phys. Rev Lett*. **85**, 3440 (2000).

29. X.-D. Zhou and W. Huebner, *Appl. Phys. Lett.* **79**, 3512 (2001).

30. F. Zhang *et al.*, *Appl. Phys. Lett.* **80**, 127 (2002).

31. L. Wu *et al.*, *Phys. Rev. B* **69**, A 125415 (2004).

32. S. Deshpande, S. Patil, S. Kuchibhatla, and S. Seal, *Appl. Phys. Lett.* **87**, 133113 (2005).

33. R.K. Hailstone *et al.*, *J. Phys. Chem. C* **113***,* 15155 (2009).

34. R. C. Cammarata, *Prog. Surf. Sci* **46** 1 (1994).

35. S. Bhatia and B.W. Sheldon, *J. Am. Ceram Soc.* **91**, 3986 (2008).

Figure Captions

Figure 1. The solid lines show the defect concentration profiles, $\hat{c}_V$ and $\hat{c}_e$, obtained by solving Eq (12) with α = 2.31, β = 2.7, χ = 0.01, and $\hat{\phi}_o$= 7.57 (conditions for $CeO_{2-\chi}$ at *T* = 1073 K and $\Delta\phi_o$ = 0.7 eV). The analogous results without considering stress contributions are shown as dashed lines.

Figure 2. (a) Predicted stress at the surface, $\sigma(0)$, as a function of the composition, χ, for $\Delta\phi_o$= 0.3 eV and 0.7 eV. (b) Contours showing constant values for $\sigma(0)$, as a function of the surface potential, $\Delta\phi_o$, and the composition, χ. The point in both plots corresponds to the case in Fig 1.

Figure 3. Predicted values of Σ_{SC} obtained from Eq. (13), by solving Eq. (12) with α = 2.31 and β = 2.7, for $\Delta\phi_o$ values of 0.3 eV ($\hat{\phi}_o$= 3.24), 0.7 eV ($\hat{\phi}_o$= 7.57) and 1.0 eV ($\hat{\phi}_o$= 10.8). The point plotted here corresponds to the case in Fig 1.

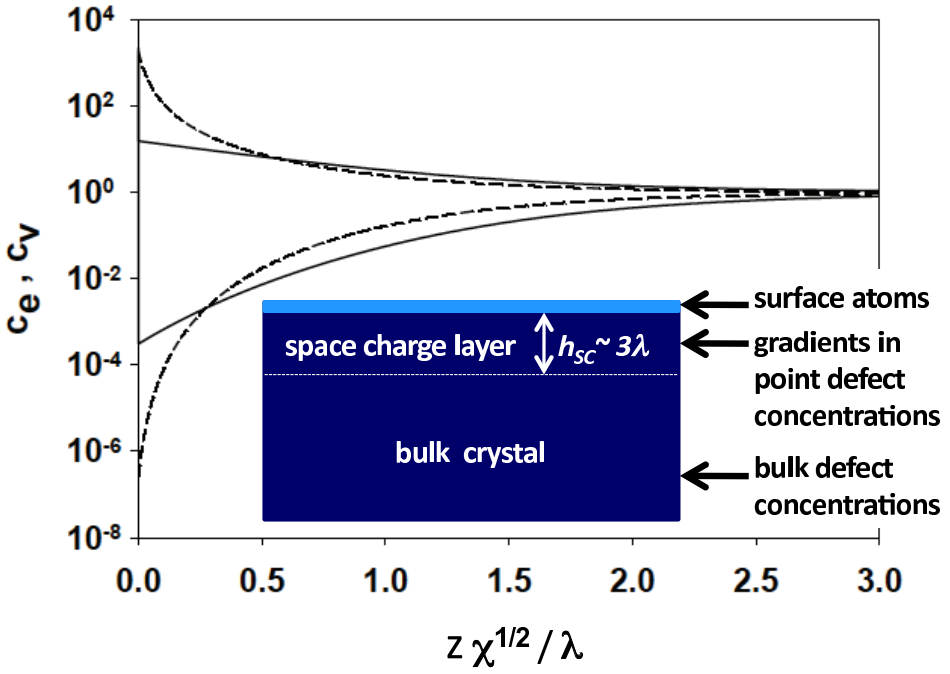

Figure 1. The solid lines show the defect concentration profiles, $\hat{c}_V$ and $\hat{c}_e$, obtained by solving Eq (12) with α = 2.31, β = 2.7, χ = 0.01, and $\hat{\phi}_o$= 7.57 (conditions for $CeO_{2-\chi}$ at T = 1073 K and $\Delta\phi_o$ = 0.7 eV). The analogous results without considering stress contributions are shown as dashed lines.

Figure 1 LB13124 18APR2011

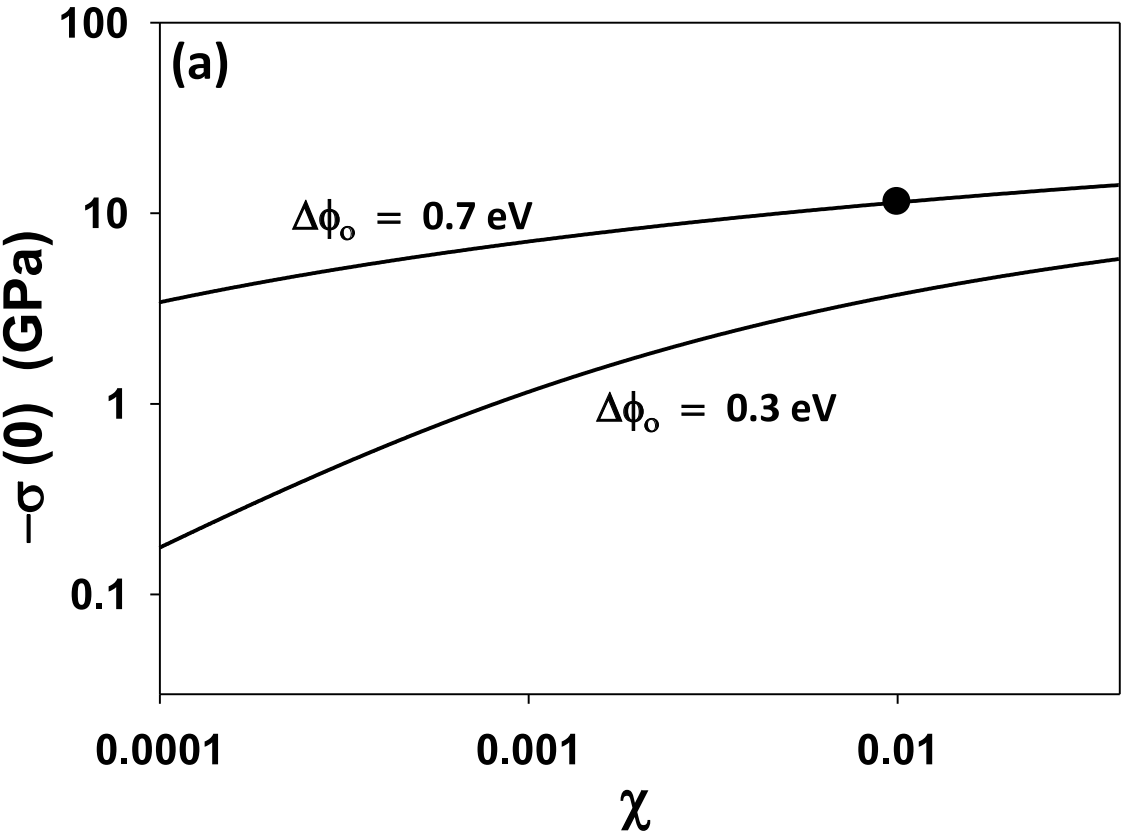

Figure 2a LB13124 18APR2011

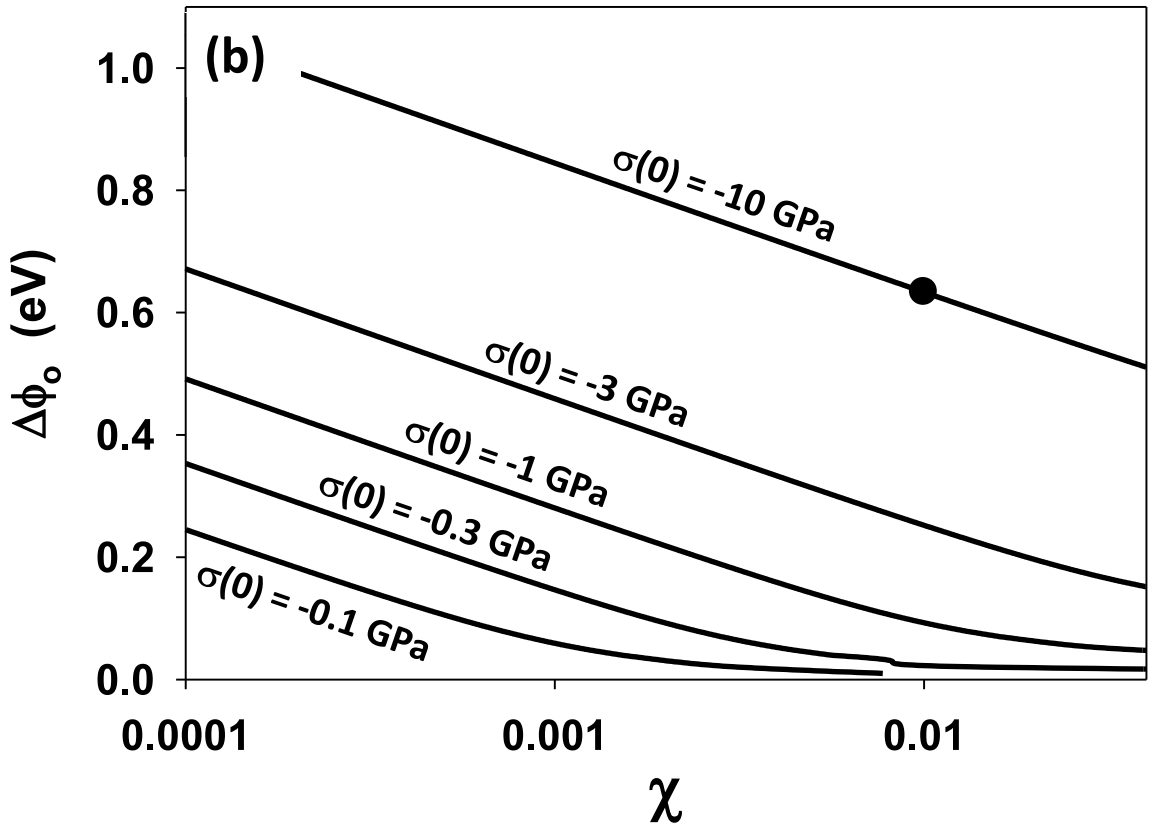

Figure 2. (a) Predicted stress at the surface, $\sigma(0)$, as a function of the composition, χ, for $\Delta\phi_o$ = 0.3 eV and 0.7 eV. (b) Contours showing constant values for $\sigma(0)$, as a function of the surface potential, $\Delta\phi_o$, and the composition, χ. The point in both plots corresponds to the case in Fig 1.

Figure 2b LB13124 18APR2011

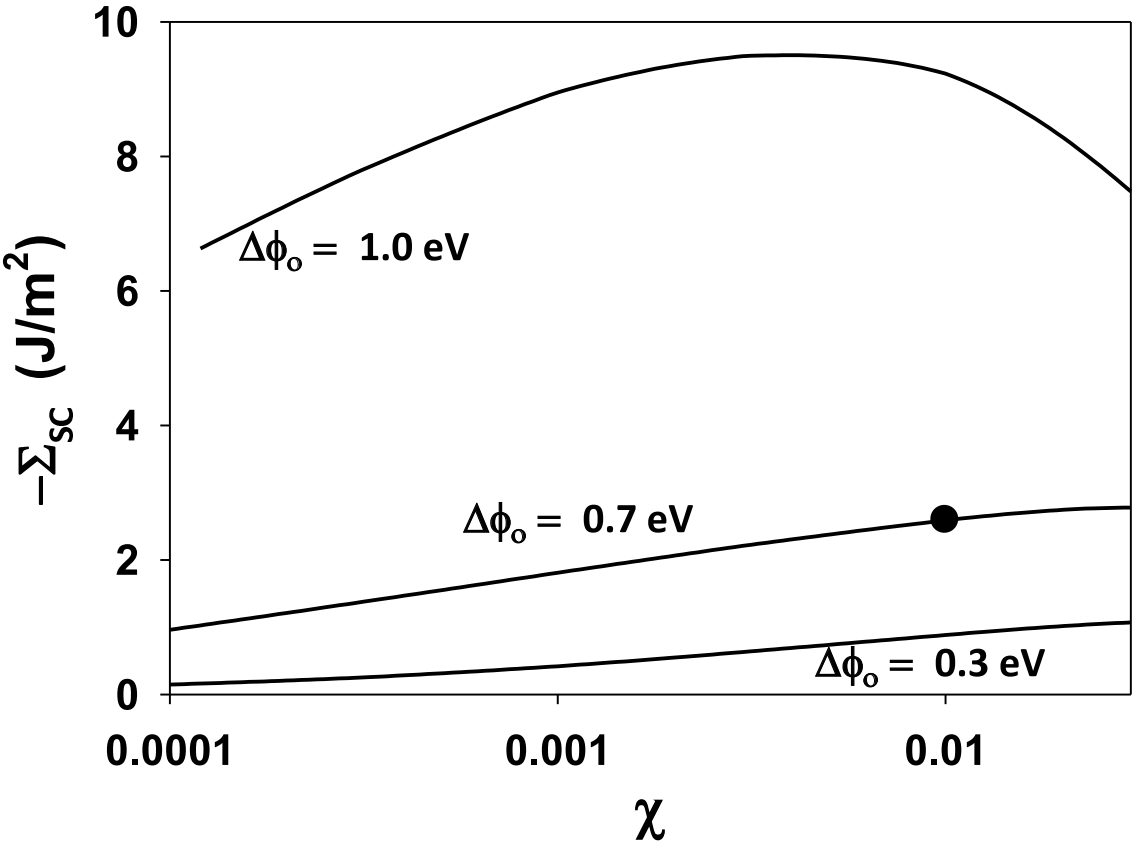

Figure 3. Predicted values of Σ_{SC} obtained from Eq. (13), by solving Eq. (12) with α = 2.31 and β = 2.7, for $\Delta\phi_o$ = 0.3 eV, $\Delta\phi_o$ = 0.7 eV, and $\Delta\phi_o$ = 1.0 eV. The point plotted here corresponds to the case in Fig 1.